



## Session VII, May 28, Thursday

L22

### SYNTHESIS AND CHARACTERISATION OF HIGH-PERFORMANCE FERROELECTRICS

Milan Klicpera

*Faculty of Mathematics and Physics, Charles University, Prague*

The development of lead-free ferroelectric materials with competitive functional performance remains a key objective in condensed matter physics and materials science. Although perovskite-based solid solutions provide a versatile platform for tuning electromechanical response, their practical utilisation is frequently hindered by limited control over compositional homogeneity, short-range structural correlations, and synthesis reproducibility.

Here, we introduce a crystal-growth-based synthesis strategy enabling the preparation of high-quality ceramics and single crystals of complex Pb-free ferroelectrics without reliance on conventional multi-step solid-state processing. Floating-zone and pedestal growth techniques are employed to achieve enhanced compositional uniformity and controlled local structural order, both critical for stabilising functional phases and maximising macroscopic response.

The approach is illustrated on representative systems, including (Ba,Ca)TiO<sub>3</sub>-based compounds and rare-earth RE<sub>2</sub>(Ti,Zr)<sub>2</sub>O<sub>7</sub> oxides. Diffraction methods combined with high-resolution microscopy reveal a high degree of structural homogeneity and well-defined crystallographic features. These structural improvements translate into reproducible and robust functional properties, comparable to or surpassing those of materials prepared by standard routes.

More generally, the proposed synthesis concept provides a transferable framework for the design and investigation of advanced ferroic systems. It supports systematic exploration of composition–structure–property relationships, particularly in regimes where local disorder and structural complexity extend beyond the scope of conventional crystallographic descriptions.

L23

### A UNIFIED STRUCTURAL FRAMEWORK FOR MODULATION AND NANOTWINNING IN Ni–Mn–Ga ALLOYS

P. Veřtát<sup>1</sup>, L. Straka<sup>1</sup>, H. Seiner<sup>2</sup>, M. Klicpera<sup>3</sup>, M. Zelený<sup>4</sup>, J. Luštinec<sup>1</sup>, O. Fabelo<sup>5</sup>, O. Heczko<sup>1</sup>

<sup>1</sup> FZU – Institute of Physics of the Czech Academy of Sciences, Prague, Czechia

<sup>2</sup> Institute of Thermomechanics of the Czech Academy of Sciences, Prague, Czechia

<sup>3</sup> Faculty of Mathematics and Physics, Charles University, Prague, Czechia

<sup>4</sup> Faculty of Mechanical Engineering, Institute of Materials Science and Engineering, Brno University of Technology, Brno, Czechia

<sup>5</sup> Institut Laue-Langevin, Grenoble, France

vertat@fzu.cz

Magnetically induced reorientation in Ni–Mn–Ga-based single crystals represents a unique paradigm of material deformation, where the crystal microstructure is manipulated through magnetically driven twin boundary motion, resulting in a giant magnetic-field-induced strain. The extraordinary mobility of twin boundaries in its martensitic phases, particularly high in the five-layered modulated martensite [1], fundamentally relies on the complex structure. Traditionally, the Ni–Mn–Ga martensite structure has been viewed through two contrasting descriptions: traditional continuous wave modulation [2] and discrete adaptive (nano)twinning [3]. Recently, we have built a unified structural framework that seamlessly bridges both distinct perspectives.

Using single-crystal neutron and X-ray diffraction, we tracked the structural evolution with temperature in several off-stoichiometric Ni–Mn–Ga alloys. We revealed that the modulation is anharmonic evidenced by an unusually rich spectrum of high-order satellite reflections and evolves continuously from a commensurate five-layered state near the martensitic transformation to an incommensurate state upon cooling [4]. Importantly, this evolution is accompanied by dramatic changes in shear stability: the shear elastic constant exhibits anomalous behaviour, indicating an extraordinary softness to the forces perpendicular to the modulation vector. Near the martensitic transformation, Ni–Mn–Ga is one of the most anisotropic metallic materials ever reported [5].

By mapping the diffraction-validated, complex anharmonic modulation onto a discrete basal-plane stacking sequence, we demonstrate that the evolving incommensurability naturally produces periodic nanodomains. Furthermore, upon cooling, the incommensurate modulation locks into various stable long-period commensurate states, whose orthorhombic unit cells simultaneously incorporate the  $a/b$ -nanotwin boundaries [6].

Since subtle dynamic shifts in the modulation phase project directly onto discrete microstructural changes in Ni–Mn–Ga, our findings also suggest that phasons—collective acoustic-like excitations in incommensurate crystals—can mediate the microstructural rearrangements with minimal required energy. Ultimately, our work not only resolves the long-standing modulation-nanotwinning duality, but also points towards the phason-driven lattice dynamics as a potentially crucial ingredient in the fundamental mechanism underlying the exceptional twin-boundary mobility in Ni–Mn–Ga-based functional materials.

1. O. Heczko, V. Kopecký, A. Sozinov, L. Straka, *Appl. Phys. Lett.* **103**, (2013) 072405.
2. T. Janssen, A. Janner, A. Looijenga-Vos, P.M. de Wolff, in *International Tables for Crystallography, Volume C: Mathematical, physical and chemical tables*, (Springer, Dordrecht), 2006, pp. 907-955.
3. A.G. Khachatryan, S.M. Shapiro, S. Semenovskaya, *Phys. Rev. B.* **43**, (1991) 10832-10843.
4. P. Veřtát, M. Klicpera, O. Fabelo, O. Heczko, L. Straka, *Scr. Mater.* **252**, (2024) 116251.
5. K. Repčák, P. Stoklasová, T. Grabec, P. Sedlák, J. Olejňák, M. Vinogradova, A. Sozinov, P. Veřtát, L. Straka, O. Heczko, H. Seiner, *Adv. Mater.* **36**, (2024), 2406672.
6. P. Veřtát, M. Zelený, A. Sozinov, M. Klicpera, O. Fabelo, R. Chulist, M. Vinogradova, P. Sedlák, H. Seiner, O. Heczko, L. Straka, ArXiv:2503.04379 (2025) (under review in *Acta Mater.*).

*This work was supported by the Ferroic Multifunctionalities project, supported by the Ministry of Education, Youth, and Sports of the Czech Republic [Project No. CZ.02.01.01/00/22\_008/0004591], co-funded by the European Union.*

**L24**

## IN SITU SYNCHROTRON X-RAY DIFFRACTION STUDY OF THE EVOLUTION OF PARTICLES AND THE TRANSITION REGION DURING HEATING

J. Šmilauerová, J. Kozlík, J. Dittrich, V. Holý

Faculty of Mathematics and Physics, Charles University, Ke Karlovu 5, 121 16, Prague, Czech Republic  
jana.smilauerova@matfyz.cuni.cz

The transformation in metastable  $\beta$ -Ti alloys plays a central role in controlling mechanical properties and lattice instabilities. Nanoscale particles form by a shuffle mechanism that can be formally described as a collapse of two neighbouring (111) planes of the body-centred cubic matrix toward their intermediate position, while the next (111) plane remains unchanged. Repeating this shuffle pattern gives rise to the hexagonal structure of the phase particles [1]. At elevated temperatures, the phase evolves further via a diffusion-assisted, displacement-controlled process in which alloying elements are rejected from the particles into the surrounding matrix, while the collapse of the (111) planes proceeds simultaneously [2]. An important aspect of the transformation is that the interface between the two phases is not sharp; instead, the degree of (111) plane collapse progresses gradually in the transition region between  $\beta$  and  $\beta'$ . Earlier work has shown that specific reflections are systematically absent in both  $\beta$  and  $\beta'$  lattices but are allowed in regions of incomplete collapse, providing diffraction signatures of the transition region.

Using in situ high-energy synchrotron X-ray diffraction, we track the evolution of  $\beta$  and transitional-phase peaks during controlled heating of a single-crystalline  $\beta$ -Ti sample (Ti-15 wt.% Mo). By analysing integrated intensities and peak shapes in selected regions of reciprocal space (see Figure 1), we determine temperature-dependent particle sizes and quantify the relative thickness of the transi-

tion region using a model based on ellipsoidal particles with a diffuse interface, in which the degree of collapse changes smoothly from ideal  $\beta$  to ideal  $\beta'$  structure.

The thermal evolution of the phase proceeds in several distinct stages. Between room temperature and approximately 250 °C, the phase partially dissolves, as indicated by a simultaneous decrease in both the number and size of particles. In the temperature range from about 250 °C to 420 °C, the remaining particles undergo pronounced growth while their total number continues to decrease, resulting in a sharp increase in the integrated intensity. Between 420 °C and 530 °C, the particle sizes remain approximately constant, but the ongoing reduction in particle number leads to a gradual decrease in the integrated intensity. Above roughly 530 °C, as the phase approaches its solvus temperature, a rapid reduction in particle size signals the final dissolution of  $\beta$ .

The evolution of the transition region is more difficult to quantify due to the intrinsically weak intensity of the corresponding diffraction peaks. Nevertheless, the integrated intensity of the transition-region peaks remains approximately constant over most of the temperature range, with a modest increase accompanying the rapid growth of particles and a pronounced decrease coinciding with their dissolution above 530 °C. Analysis of the transition-region width relative to the  $\beta$ -particle size reveals an initial broadening during the low-temperature dis-

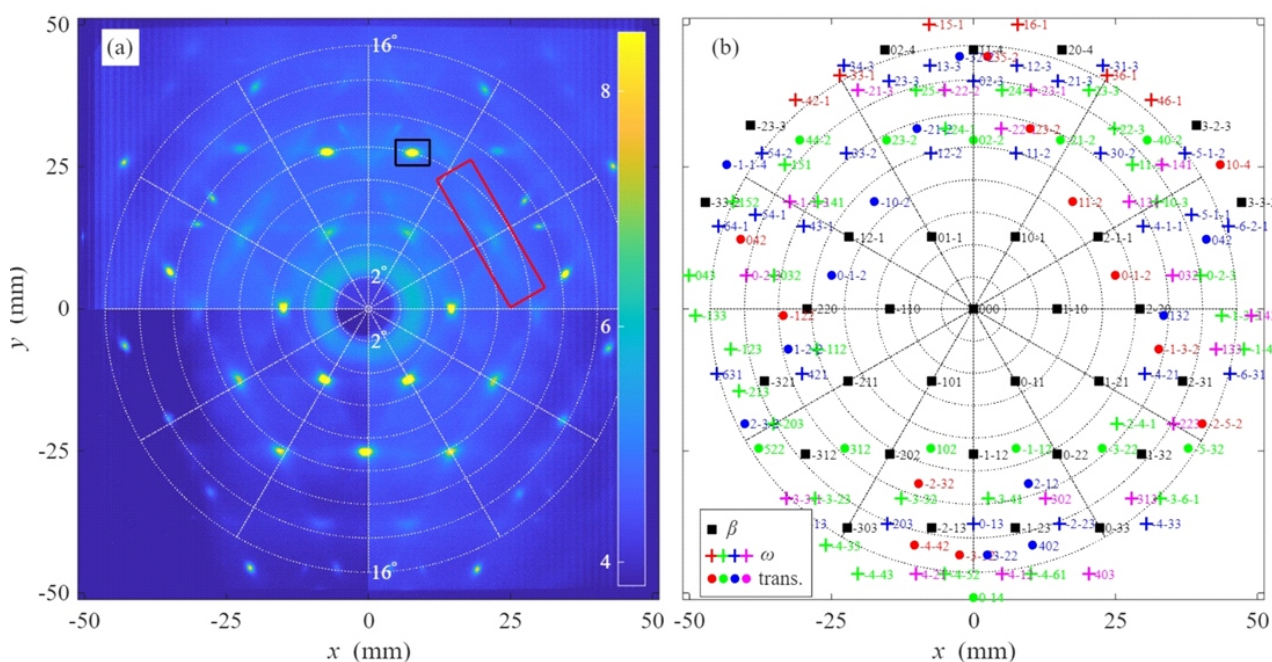


**Figure 1.** An example of the reciprocal-space maps analysed in this study. (a) Detector image recorded at room temperature; black and red rectangles indicate the regions of interest round and transition-region peaks, respectively. (b) Calculated positions of  $\beta$ ,  $\omega$  and transition-region peaks. The four colours of the  $\omega$  and transition maxima correspond to four crystallographically equivalent  $\omega$  families.

solution stage, followed by a narrowing that coincides with the temperature interval of rapid  $\omega$ -particle growth.

1. D. De Fontaine, *Acta Metallurgica*, **18**, (1970), 275.
2. T. W. Duerig, G. T. Terlinde, J. C. Williams, *The  $\omega$ -phase reaction in titanium alloys in Titanium '80 Science & Technology - Proceedings of the 4th Int'l Conference on Titanium*, (1980), 1299.
3. J. Šmilauerová, P. Harcuba, D. Kriegner, V. Holý, *Journal of Applied Crystallography*, **50**, (2017), 283.

*This work was supported by a project of the Czech Science Foundation (GACR) project no. 23-09637L. Single crystal growth was performed in MGML (<http://mgml.eu/>), which is supported by the Czech Research Infrastructures program (project No. LM LM2023065). The authors would like to acknowledge ESRF for providing beamtime through the experiment MA6531 (<https://doi.org/10.1515/ESRF-ES-2243238109>) and beamline staff at ID11 beamline for assistance during the experiment.*

**Session VIII, May 28, Thursday**

L25

**HIGH-THROUGHPUT RESEARCH OF HIGH ENTROPY ALLOYS USING LABORATORY XRD****František Lukáč<sup>1</sup>, Jiří Kozlík<sup>2</sup>, Mariano Casas-Luna<sup>2</sup>, Josef Stráský<sup>2</sup>**<sup>1</sup>*Institute of Plasma Physics of the Czech Academy of Sciences, U Slovanky 2525/1a, Prague 182 00, Czechia*<sup>2</sup>*Charles University, Faculty of Mathematics and Physics, Department of Physics of Materials, Ke Karlovu 5, Prague 121 16, Czechia*

This study investigates phase equilibria within the Al–Ti–Nb–Zr–Ta refractory complex concentrated alloy (RCCA) system using a high-throughput combinatorial experimental approach. A pseudo-ternary section was fabricated via a honeycomb-type powder metallurgy design, consolidated through spark plasma sintering (SPS), and subjected to homogenization at 1400°C for 168 hours. Phase constitution and chemical partitioning were characterized using an integrated suite of SEM/EDS, EBSD, and TEM, supported by a custom EDS phase-clustering workflow [1]. Structural analysis was further refined through X-ray diffraction (XRD) utilizing both 1D linear and 2D area detectors; the latter proved essential for identifying significant preferential orientation (texture) and grain coarsening induced by the prolonged high-temperature annealing.

Equilibrium microstructures across the sampled compositions consisted primarily of BCC and B2 phases, with nanoscale precipitates forming in Zr- and Ta-rich regions. Experimental phase compositions were compared with CALPHAD predictions, revealing consistent systematic deviations that highlight current limitations in multicomponent thermodynamic databases. These results provide critical insights into the phase stability and microstructural trends of the Al–Ti–Nb–Zr–Ta system while demonstrating the efficacy of high-throughput methods and multidimensional XRD analysis in mapping complex alloy spaces.

- [1] J. Kozlík, E. Jača, M. Vilémová, F. Lukáč, T. Chráska, J. Stráský, Honeycomb sample design for high-throughput preparation of RCCAs, *Mater. Lett.* 398 (2025) 138957. <https://doi.org/10.1016/j.matlet.2025.138957>.

L26

**UNIAXIAL-STRAIN TUNING OF THE METAL-INSULATOR TRANSITION IN -(BEDT-TTF)<sub>2</sub>Cu[N(CN)<sub>2</sub>]Br****P. Doležal<sup>1,2</sup>, T. Pinter<sup>1</sup>, K. Boniecki<sup>1</sup>, A. Chen<sup>1</sup>, R. Saito<sup>3</sup>, A Kawamoto<sup>3</sup>, A. Pustogow<sup>1</sup>**<sup>1</sup>*TU Wien, Institute of Solid State Physics, 1040, Vienna, Austria*<sup>2</sup>*Charles University, Dep. of Condensed Matter Physics, 121 16, Prague, Czech Republic*<sup>3</sup>*Hokkaido University, Dep. of Physics, Graduate School of Sci., 060-0810, Sapporo, Japan*  
*petr.dolezal@matfyz.cuni.cz*

The organic charge transfer salts are intensely studied compounds for their unique physical properties, in particular the single-band Mott metal-insulator transition and frustrated magnetism. This is the reason why these compounds serve as an experimental playground for the theoretical investigation of Hubbard model on the half-filled triangular lattice of quantum-spin-liquid candidates [1]. The layers of cations and anions with weak bonding create the quasi-2D character and enable large compressibility which allows modification of their physical properties in a large area in the phase diagram. It can be realized by application of hydrostatic or uniaxial pressure or by chemical substitution. While these mechanical properties are advantageous for tuning the physical properties, on the other side the performance of such experiments is very challenging because these compounds are also very brittle. Only very recently

the in situ uniaxial-strain tuning of correlations and frustration strength within a single crystal became accessible [2].

Here we report the first controlled tuning of the Mott transition via uniaxial strain on free-standing organic single crystals in a piezoelectric strain cell. This versatile tool enables us to tune through the metal-insulator transition in a quasi-continuous fashion at cryogenic temperatures, as shown in Fig. 1. Due to negative chemical pressure upon substitution of <sup>1</sup>H by <sup>2</sup>D this compound exhibits Mott-insulating behaviour with an antiferromagnetic ground state at ambient pressure [3]. Here, we modified the strength of electronic correlations by uniaxial compression, yielding metallic and superconducting properties (Fig. 1a,b).

1. A. Pustogow, M. Bories, A. Löhle, R. Rösslhuber, E. Zhukova, B. Gorshunov, S. Tomić, J. A. Schlueter, R. Hübner, T. Hiramatsu, Y. Yoshida, G. Saito, R. Kato,



- T.-H. Lee, V. Dobrosavljević, S. Fratini, M. Dressel *Nature Materials*, **17**, (2018), 1694.
2. J. Wang, M. Spitaler, Y.-S. Su<sup>1</sup>, K. M. Zoch, C. Krellner, P. Puphal, S. E. Brown, and A. Pustogow, *Phys. Rev. Lett.*
3. H. Ito, T. Ishiguro, T. Kondo, G. Saito, *J. Phys. Soc. Jpn.* **69**, (2000), 290-291.

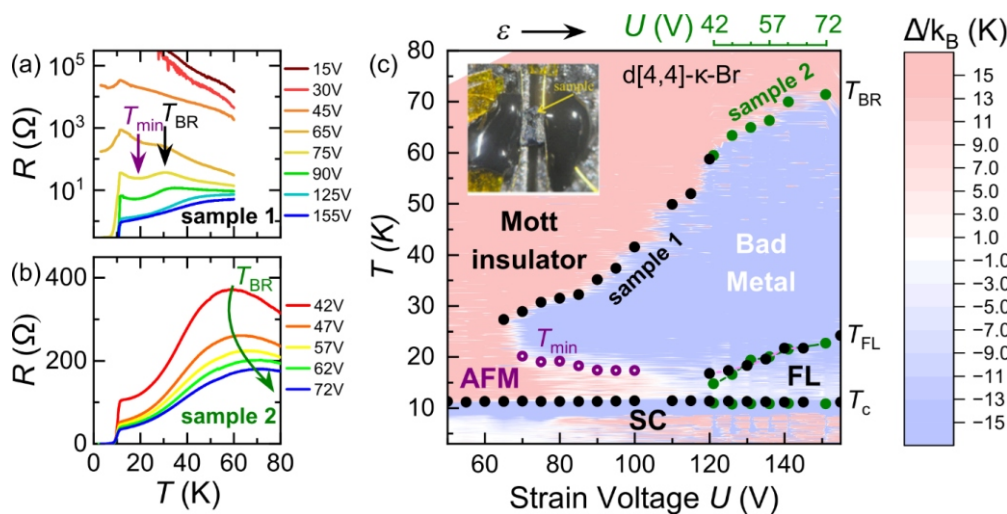


Figure 1. a), b) Electrical resistivity of d[4,4]- k-Br under uniaxial strain. c) The resulting phase diagram.

131 (2023), 256501.

L27

## POLYMORPHISM OF HELICENES STUDIED BY DSC AND VT-XRD

V. Pokorný<sup>1</sup>, J. Obuch<sup>1</sup>, Š. Kocian<sup>2</sup>, V. Štejfa<sup>2</sup>

<sup>1</sup>Institute of Macromolecular Chemistry, Czech Academy of Sciences, Heyrovského nám. 2, 162 00, Prague 6, Czech Republic

<sup>2</sup>Department of Physical Chemistry, University of Chemistry and Technology, Prague, Technická 5, 166 28 Prague 6, Czech Republic  
pokorny@imc.cas.cz

Helicenes are a class of inherently chiral,  $\pi$ -conjugated polycyclic aromatic hydrocarbons characterized by their helical structures and unique chiroptical properties [1]. Their rigid yet non-planar geometry makes them valuable model systems for investigating the relationship between molecular shape and crystal packing [2]. In the solid state, subtle variations in intermolecular interactions can lead to polymorphism, which can significantly influence the physical properties of these materials. Despite extensive crystallographic studies of helicenes [3], polymorphism in shorter homologues such as [4]- and [5]-helicene remains insufficiently explored.

New polymorphs of [4]-helicene and [5]-helicene were identified by differential scanning calorimetry (DSC, TA Q2000) and characterized by variable-temperature powder X-ray diffraction (VT-PXRD; Anton Paar XRDynamic 500 equipped with a TTK600 temperature chamber, rotating 0.5 mm capillary). Temperature-dependent PXRD measurements were used to monitor phase transitions and isolate the new forms. Crystal structures were determined from powder data by indexing and structure solution using FOX, followed by Rietveld refinement in Jana2020.

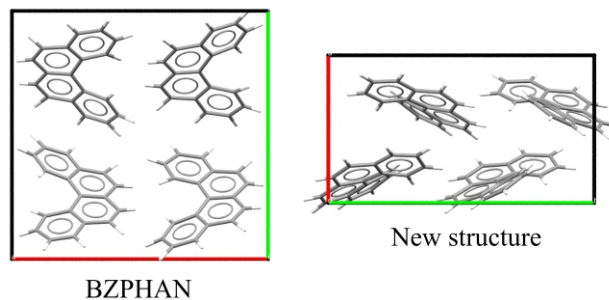


Figure 1. Comparison of crystal packing in different polymorphs of [4]-helicene.

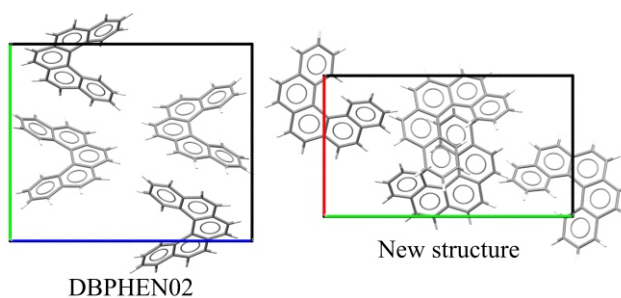


Figure 2. Comparison of crystal packing in different polymorphs of [5]-helicene.

**Table 1.** Parameters of previously known and newly determined structures of [4]-helicene and [5]-helicene.<sup>a</sup>

| polymorph <sup>b</sup> | <i>a</i> / Å  | <i>b</i> / Å  | <i>c</i> / Å | /         | Z         | Space group                                   | T <sub>melt</sub> / °C |
|------------------------|---------------|---------------|--------------|-----------|-----------|---|------------------------|
| [4] helicene           |               |               |              |           |           |   |                        |
| BZPHAN                 | 14.660        | 14.157        | 5.785        | 90        | 4         | P2 <sub>1</sub> 2 <sub>1</sub> 2 <sub>1</sub> | 66                     |
| <b>New</b>             | <b>14.497</b> | <b>10.400</b> | <b>8.025</b> | <b>90</b> | <b>4</b>  | <b>Pbc2<sub>1</sub></b>                       | <b>45</b>              |
| [5] helicene           |               |               |              |           |           |   |                        |
| DPHEN02                | 5.815         | 14.178        | 17.498       | 94.41     | 4         | P2 <sub>1</sub> /c                            | 155                    |
| DPHEN03                | 26.013        | 8.898         | 19.494       | 103.94    | 12        | A2/a  | 178                    |
| DPHEN05                | 20.307        | 8.977         | 7.756        | 90        | 4         | Pbcn  | n.d. <sup>c</sup>      |
| <b>New</b>             | <b>9.924</b>  | <b>17.536</b> | <b>8.395</b> | <b>90</b> | <b>40</b> | <b>Pna2<sub>1</sub></b>                       | <b>162</b>             |

<sup>a</sup> parameters *a* and *b* are 90° in all cases. *c* = 90° indicates an orthorhombic cell.

<sup>b</sup> identified by the CSD refcode, if available.

<sup>c</sup>n.d. stands for not determined.

An overview of previously reported and newly identified polymorphs is given in Table 1. While the molecular conformation remains unchanged across all structures, significant differences are observed in crystal packing (see Figures 1 and 2). These packing variations correlate with differences in melting temperature, suggesting changes in lattice stability between polymorphs.

These findings extend the known structural diversity of helicenes and support their use as model systems for packing-driven polymorphism in rigid  $\pi$ -conjugated molecules.

1. M. Cei, L. Di Bari, F. Zinna, *Chirality*, **35**, (2003), pp. 192-210.

2. Y. Shen, C. Shen, *Chem. Rev.*, **112**, (2012), pp. 1463-1535.

3. J. A. Schmidt, E. H. Wolpert, G. M. Sparrow, E. R. Johnson, K. E. Jelfs, *Cryst. Growth Des.*, **23**, (2023), pp. 8909-8917.

*We acknowledge financial support from the Czech Science Foundation (project No. 24-15057L). We would like to thank Michal Šámal from UOCHB for the synthesis of Helicene samples.*



P2

## EFFECT OF QUARTZ AND NANOSILICA ON THE HYDRATION OF LC<sup>3</sup> CEMENT

S. Švarcová<sup>1</sup>, P. Bezdička<sup>1</sup>, L. Scheinherrová<sup>2</sup>, M. Breníková<sup>2</sup>, M. Keppert<sup>2</sup>

<sup>1</sup>Institute of inorganic chemistry of the Czech academy of sciences v.v.i., Husinec-Řež 1001, 250 68 Husinec-Řež

<sup>2</sup>Department of materials engineering and chemistry, Faculty of civil engineering, Czech technical university in Prague, Thákurova 7, 166 29 Praha 6  
svarcova@jic.cas.cz

Limestone calcined clay cements (LC<sup>3</sup>) are supposed to be perspective low-carbon alternative to conventional ordinary Portland cement (OPC) and blended cements. [1] LC<sup>3</sup> cements typically contain 50 % (or less) of Portland clinker, 30 % of calcined clay (here metakaolin), 15 % of fine ground limestone and 5 % of gypsum. The reduced environmental impact lies obviously in the lower content of Portland clinker but contrary, the low content of clinker is responsible for the slower concrete strength gain which is highly unfavourable property in the current construction industry. Hence a way for acceleration of LC<sup>3</sup> hydration and strengthening is searched. There is a lot of acceleration admixtures well established in OPC based concrete such as CaCl<sub>2</sub>, Ca(NO<sub>3</sub>)<sub>2</sub> or water glass. [2] However, their applicability in LC<sup>3</sup> systems may be limited compared to OPC.

The present research aims to evaluate the possible hydration acceleration in LC<sup>3</sup> by means of fine grained quartz (Q) and amorphous nanosilica (nS). These admixtures were dosed in amount of 3 % by clinker mass to LC<sup>3</sup> system of the common composition given above. The effect of addition of these admixtures was evaluated by isothermal calorimetry (20 °C), by determination of compressive strength in the age of 1 day (paste w/c 0.37, water reducing admixture was used to maintain proper workability) and finally by *in situ* XRPD obtained on the fresh paste, placed on PEEK foil, and measured in reflection mode in 1 hour period.

The shape of isothermal calorimetry heat flow curve of plain LC<sup>3</sup> (Fig. 1) is very similar to conventional OPC systems; the strongly exothermic C<sub>3</sub>A hydration starts immediately after adding of water (time 0), then an induction

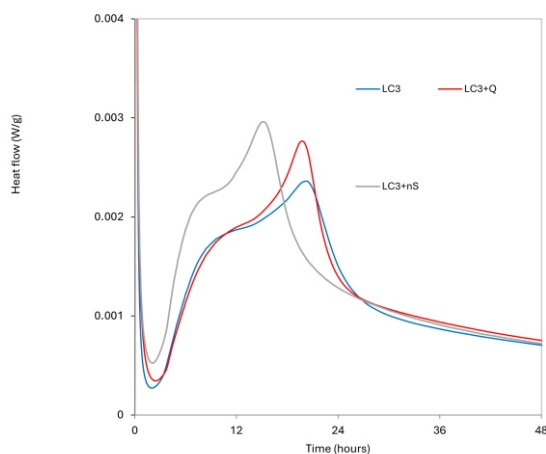


Figure 1. Hydration heat flow.

Table 1. Compressive strength in 24 hours.

| Sample                     | LC3 | LC3+Q | LC+nS |
|----------------------------|-----|-------|-------|
| Compressive strength (MPa) | 4.5 | 4.7   | 7.9   |

(low heat flow) period appears and at about 3 hours, intensive heat evolution caused by C<sub>3</sub>S hydration starts. When quartz was added, the heat flow curve featured just a small change while nanosilica caused more pronounced increase of hydration heat as well as certain shortening of the induction period. This behaviour was confirmed also by the compressive strength measurement (Tab. 1) – quartz system reached the same value as plain LC<sup>3</sup>, while nanosilica caused significant increase of the 1-day strength.

The *in situ* XRPD was used in order to explain how the quartz and nanosilica admixtures influence the hydration course. The XRPD patterns obtained in time of hydration 4 hours (initial part of main hydration peak; Fig. 2) are practically equal; the only observed crystalline hydration product in all systems was AFt phase (ettringite is the most prominent representative of AFt). Other observed phases come from the raw materials of LC<sup>3</sup>. After 12 hours (Fig. 3; intensive hydration heat flow) portlandite (Por, Ca(OH)<sub>2</sub>) appeared as another important hydration product. Portlandite is related to the C<sub>3</sub>S hydration. The intensity of portlandite diffraction at 21° was the highest in the plain LC<sup>3</sup>, while the both admixtures reduced significantly its height. It implies that siliceous admixtures promoted the consumption of portlandite in the pozzolanic reaction with

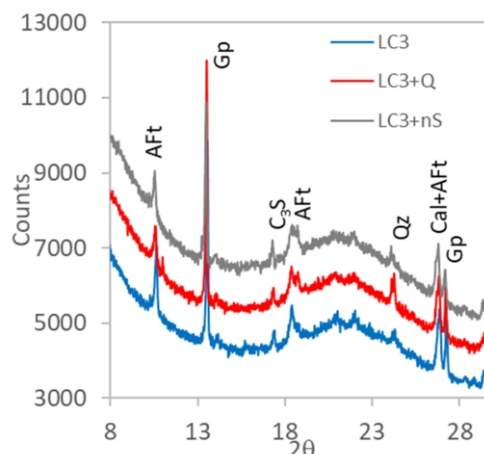


Figure 2. XRPD patterns in 4 hours.

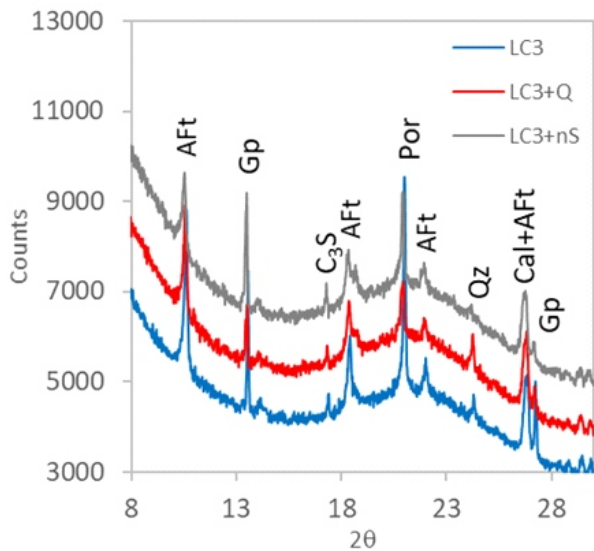


Figure 3. XRPD patterns in 12 hours.

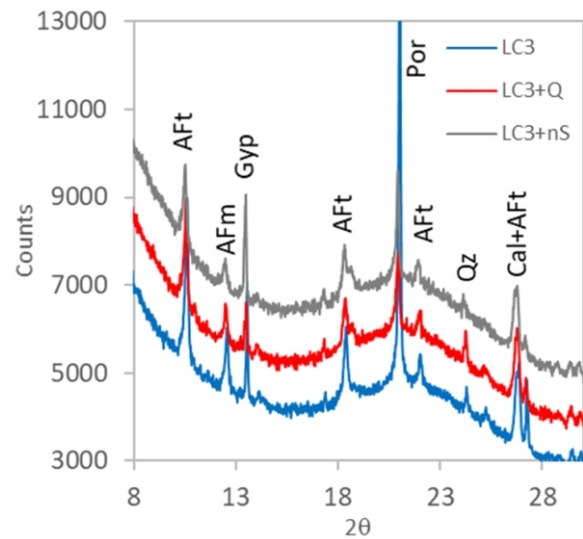


Figure 4. XRPD patterns in 24 hours.

metakaolin, when compared with the plain  $LC^3$ . There are also observable changes in gypsum (Gp) and AFt diffractions –  $SiO_2$  additives seems to reduce the AFt formation. The 24 hours data (end of the main hydration peak; Fig. 4) confirmed these trends, intensity of portlandite diffraction was again much higher in reference  $LC^3$  without additives. AFm phase (generic formula  $3CaO \cdot (Al,Fe)_2O_3 \cdot CaX_y \cdot nH_2O$ ) appeared at 24 h as product of AFt partial conversion (the peak at main hydration peak is supposed to be related to the AFm crystallization).

It can be concluded that both  $SiO_2$  admixtures promoted the pozzolanic reaction between  $Ca(OH)_2$  and metakaolin in  $LC^3$  but only nanosilica caused substantial increase of compressive strength. It may be due to the involvement of nanosilica in the pozzolanic reaction by itself (besides accelerating the reaction between  $Ca(OH)_2$  and metakaolin). The content of nanosilica is low compared to metakaolin but it may be assumed that it is much more reactive thank to its high specific surface area and low particle size.

1. K. Scrivener, F. Martirena, S. Bishnoi, S Maity, *Cem. Conc. Res.*, **114**, (2018), 49-56.
2. T. Dorn, O. Blask, D. Stephan, *Con. Build. Mat.*, **323**, (2022), 126554.

*This work has been supported by Czech Science Foundation under project Nr. 25-15200S “Opportunities for increasing low early strength of eco-friendly blended cements through innovative additives and nanomaterials”.*